Journal of Materials Chemistry A

Accepted Manuscript

ROYAL SOCIETY OF CHEMISTRY

www.rsc.org/materialsA

Journal of Materials Chemistry A

COMMUNICATION

Conformally Deposited NiO on a Hierarchical Carbon Support for High-Power and Durable Asymmetric Supercapacitor

Received 00th January 20xx,
Accepted 00th January 20xx

DOI: 10.1039/x0xx00000x

www.rsc.org/

Cao Guan[a], Yadong Wang[b], Yating Hu[a], Jilei Liu[c], Kuan Hung Ho[a], Wei Zhao[d], Zhanxi Fan[d], Zexiang Shen[c], Hua Zhang[d], John Wang[a]**

Metal oxide based supercapacitors can provide much higher energy densities as compared with carbon-based ones. However, metal oxides are usually suffered from low power densities together with poor cycle life, which is a big barrier for their practical applications. In this work, purposely confined NiO nanoparticles has been deposited uniformly on a three-dimensional graphite foam-carbon nanotube forest substrate, giving rise to a well-integrated free-standing electrode (GF-CNT@NiO) with strong synergetic effects generated from nickel oxide and carbon support. The electrode with 57.6% mass content of NiO delievers a high specific capacity of 196.5 mAh g^{-1} and excellent cycling stability for 30 000 cycles. When coupled with a graphene-CNT paper anode, an asymmetric supercapacitor (GF-CNT@NiO//G-CNT) is assembled, which demonstrates excellent cycling ability (only 18.3% of the capacitance drop after 30 000 cycles) and high power density (1.06-7.14 kW kg^{-1}), suggesting its great promise for advanced supercapacitors.

Searching for powerful and safe energy storage devices with high energy density, high power density and long cycling life has been an important topic in the current energy-concerned society.[1-4] Supercapacitors, which can provide higher power density than that of batteries and higher energy density than that of dialetric capacitors, have been widely utilized in hybrid electric vehicles, emergency power supply, and portable electronics.[5-8] A typical asymmetric supercapacitor is composed of one battey-type electrode for high energy and one doule-layer-type electrode for high power. As been well known, the electrochemical hebaviour is largely related to the electrode materials, thus considerable efforts have been devoted to search for high quality electrode materials.[9] As promising cathode materials, nickel oxides (and hydroxides) have received much research attention because of their high energy density, environmental compatibility, and low-cost compared to RuO_2.[10-13] However, the largely insulating nature and the limited kenetics of nickel oxide usually lead to low power density and poor cycling ability.[14, 15] Fabricating nickel oxide with proper nanostructures and integrating it with conductive carbon matrix have been shown promising for high-energy electrodes.[16-20] With this objective, several nickel oxide based nanostructures, such as hollow spheres, nanowire arrays and core-shell arrays, and their combination with different carbon materials have been demonstrated with improved electrochemical perforamce.[11, 21-25] In addition, recent research work on supercapacitors have shown merits to fabricate binder-free and addictive-free electrode,[3, 26-28] which can effectively improve the electrical conductivity and cycling ability of the energy storage devices. Nevertheless, it remains a big challenge to develop high-performance NiO electrodes with satisfactory high power density and excellent cycling durability.

In this work, we develop a hierarchical graphite foam-carbon nanotube forest substrate (GF-CNT) and conformal coat its surface with refined NiO nanoparticles by atomic layer deposition(ALD). The thus obtained GF-CNT@NiO can be well served as the cathode of high-power asymmetric supercapacitors. In the electrode design, the GF-CNT has been chosen as a light, stable and flexible carbon substrate with high electric conductivity, and ALD NiO with high uniformity can express high capacity and long-time cycling ability in electrochemical application. By coupling with a flexible graphene/carbon nanotube paper (noted as G-CNT) anode, a flexible GF-CNT@NiO//G-CNT asymmetric supercapacitor has been assembled and shown very promising electrochemical behavior: it can deliver a maximum power density of 7.14 kW kg^{-1} and a maxmium energy density of 23.4 Wh kg^{-1} (based on the total electrode mass), and more than 80% of the capacity

[a] *Department of Materials Science and Engineering, National University of Singapore, 117574 Singapore.*
E-mail: mseqc@nus.edu.sg; msewangj@nus.edu.sg
[b] *School of Engineering, Nanyang Polytechnic, 569830 Singapore*
[c] *School of Physical and Mathematical Sciences, Nanyang Technological University, 637371 Singapore*
[d] *School of Materials Science and Engineering, Nanyang Technological University, 639798 Singapore*

† Footnotes relating to the title and/or authors should appear here.
Electronic Supplementary Information (ESI) available: [details of any supplementary information available should be included here]. See DOI: 10.1039/x0xx00000x

can be maintained even after 30 000 cycles of charge-discharge. This work also provides a promising strategy to rationally construct novel metal oxide/carbon composites for high-performance flexible energy storage devices.

GF-CNT@NiO was developed as a free-standing electrode *via* a two-step process. Firstly, GF-CNTs were grown *via* a chemical vapor deposition method according to a previously published report.[29] In the second step, a uniform and comformal layer of refined NiO nanoparticles was deposited on the GF-CNT surface by ALD, using Nickelocene ($NiCp_2$) and O_3 as precursors (Details in Method Section).[30, 31] SEM images reveal that the hierarchical structure of GF-CNT is well maintained after the NiO deposition (Figure 1a -b), and the enlarged view in Figure 1c clearly shows the CNT surface has been uniformly coated with many nanoparticles, confirming the successful construction of carbon support with metal oxide nanoparticles. Since the amount of deposited NiO can be simply controlled by ALD cycles[32, 33], in present work NiO with 300, 600, and 900 ALD cycles have been deposited on the GF-CNT, noted as GF-CNT@300NiO, GF-CNT@600NiO, and GF-CNT@900NiO, respectively. The growth rate of NiO on CNT is ~ 0.02 nm per cycle, which is a little faster than a similar work of NiO on graphene,[34] and it is comparable to the growth rate of Fe_2O_3 on CNT.[35]

To further study the detailed nanostructure and chemical composition of the GF-CNT@NiO, transmission electron microscopy (TEM) was performed, and the results are shown in Figure 1d-f. It is clear that NiO nanoparticles with a diameter of ~5-10 nm are uniformly assembled on the surface of CNTs (Figure 1d). Incearsing the ALD NiO cycles to 900 can enlarge the particle size to ~20 nm, and the mass loading of NiO can be increased from 51.3 % to 65.4% (Electronic Supplementary Information). Noticing ultrasonic is used during the sample preparation, the NiO nanoparticles are still tightly bonded with the CNTs. Figure 1e-f displays high-resolution TEM (HRTEM) images of CNT@NiO wih different focusing points (enlarged pictures can be also found in Electronic Supplementary Information). The lattice space of 0.34 nm clearly shows the multi-walled CNT, and lattice fringes of 0.241 nm and 0.209 nm match well with the (111) and (200) planes of NiO (JCPDS 65-5745), respectively, further verifying that the nanoparticles are highly crystallined NiO.[30] HAADF-STEM and the corresponding Energy-dispersive spectroscopy (EDS) mapping of O, C and Ni are shown in Figure 1g–i, which clearly illustrates that the Ni and O atoms are homogeneously distributed throughout the CNT, showing the conformal coating by ALD.

Figure 2a presents typical X-ray diffraction (XRD) pattern of GF-CNT@NiO. Excluding the peaks of the carbon substrate, all other diffraction peaks can be well indexed to NiO (JCPDS 65-5745), which match well as previous reports on ALD NiO.[34]XPS survey spectra of the GF-CNT@NiO is presented in Figure 2b-d (the wide range spectra is in Electronic Supplementary Information). The peaks located at 871.5 and 853.0-854.7 eV accompanied by a broad satellite peak correspond to the characteristic Ni 2p 1/2 and Ni 2p 3/2 peaks of Ni^{2+} (Figure 2b),[36, 37] and the peak of O 1s centered at 530.1 eV and 531.6 eV can be attributed to the metal oxide form (O_2^-) and surface -OH group, respectively (Figure 2c).[38] In Figure 2d, the C 1s peak at 284.6 eV illustrates the C-C bond, and the C-O and C=O bonds are also shown by the small peaks at 285.8 and 288.6 eV, respectively.[34] A detailed XPS results on all three samples(GF-CNT@300NiO, GF-CNT@600NiO, and GF-CNT@900NiO) is shown in Figure S3. From the XPS results, we found the Ni 2p spectra from all the three samples are almost the same, but in the C 1s spectra, the GF-CNT@900NiO shows less C-O and C=O bonds than the other two samples, which may result in poorer stability than those of GF-CNT@300NiO and GF-CNT@600NiO.

To evaluate the electrochemical properties of the GF-CNT@NiO as a battery-typed cathode, electrochemical tests were first carried out using a three-electrode system. A 2 M KOH solution was used as the electrolyte, and a Pt plate and an Hg/HgO were used as the counter electrode and the reference electrode, respectively (Details in Experimental Section). Figure 3a compares the cyclic voltammetry (CV) curves of the four samples (GF-CNT, GF-CNT@300NiO, GF-CNT@600NiO, and GF-CNT@900NiO) at the same scan rate of 50 mV s^{-1}. The three samples after NiO coating show apparent redox peaks in the CV curves, suggesting that reversible Faradaic reaction is involved. The redox peaks centered at ~0.4 V vs. Hg/HgO can be well attributed to the reversible reaction between Ni^{2+} and Ni^{3+} with OH^-.[11, 39-42] The enclosed area of the three samples are much larger than that of the bare GF-CNT substrate, showing the capacity is much improved. And GF-CNT@600NiO shows higher capacity than both GF-CNT@300NiO and GF-CNT@900NiO.

The same capacity trend is further revealed by the galvanostatic charge–discharge curves in Figure 3b. All the charge-discharge curves have aparent platforms, showing typical battery-typed electrchemical behavious of NiO. At the current density of 5 mA cm^{-2}, GF-CNT@600NiO shows much longer discharge times than both GF-CNT@300NiO and GF-CNT@900NiO, indicating higher capacity. As expected, the GF-CNT@600NiO exhibits more active material than GF-CNT@300NiO, which could lead to the capacity increase. But if the active material of NiO is further increased, the thicker NiO layer can retard the electrochemical reaction at high rate, which can explain the capacity decrease of GF-CNT@900NiO compared with GF-CNT@600NiO.[34, 43] In current work, GF-CNT@600NiO shows the optimized capacity.

Figure 3c shows the relationship between the capacity of the samples and the charge-discharge current densities. As been suggested recently,[44] NiO is a typical battery-type material but not a pseudocapacitive material, so in the current work, we only calculate the specific capacity (but not the specific capacitance) of the NiO electrodes. As expected, the capacity retention rates decreased with thicker NiO layer. GF-CNT@300NiO shows the best capacity retention when the current increased from 5 to 40 mA cm^{-2}, since the NiO layer is the thinnest which can maintain the fast electron/charge transfer at high rates. GF-CNT@900NiO has larger capacity than that of GF-CNT@300NiO, but only 71.5% of the capacity can be maintained when the current is increased 8 times. In contrast, GF-CNT@600NiO shows a moderate capacity retention (75.1%) with the highest capacity of 196.5 mAh g^{-1} achieved at a current of 5 mA cm^{-1}. Remarkably, the specific capacity of GF-CNT@600NiO is much

larger than most of the previouslyreported results on NiO or $Ni(OH)_2$ based materials.[10, 45-47]

To better understand the relationship of the electrochemical properties with the ALD coating thickness, electrochemical impedance spectroscopy (EIS) was conducted. Figure 3d shows the Nyquist plots for the three electrodes (GF-CNT@300NiO, GF-CNT@600NiO, and GF-CNT@900NiO), and each plot is composed with two parts: a semicircle in the high frequency regions and a straight line in the low frequency region.[48] The diameter of semicircle increases with increasing number of ALD cycles, showing the charge transfer resistance is increased with thicker NiO layer.[26] The slope of the straight line (which corresponds to the electrolyte and proton diffusion resistance) decreases a little with more ALD NiO cycles, showing thicker NiO layer can result in higher resistance for ion/proton diffusion.[49] The EIS result clearly reveals that the conductivity of the samples will be dropped with thicker NiO, which agrees well with the previous discussion that GF-CNT@300NiO shows the best rate capability.

As a key parameter to evaluate the electrochemical performance, the cycling ability of GF-CNT@NiO is further studied. As shown in Figure 3e, all the three samples illustrate excellent cycling ability at the current density of 20 mA cm^{-2}. The capacitance of GF-CNT@900NiO increased to ~125% at the first 10 000 cycles, which can be due to the activation of the large-sized NiO.[7, 10, 39] After 30 000 cycles of charge-discharge, 94.6%, 83.5%, and 77.6% of capacitance can be maintained for GF-CNT@300NiO, GF-CNT@600NiO, and GF-CNT@900NiO, respectively. The cycling ability is among the best results achieved so far from NiO-based electrodes.[21, 22, 46] It is noted that there was no apparent change in the morphology of the GF-CNT@NiO electrode after 30 000 cycles, as depicted in Figure 3f, which further demonstrates the excellent cycling stability. The digit photos of the electrodes before and after testing, and the TEM image of the electrode after cycling test are shown in Electronic Supplementary Information. The cycling results confirm the merits of the stable hierarchical GF-CNT substrate, and the stable structure of CNT coated with confined nanosized crystalline NiO.

To demonstrate the feasibility of the as-prepared GF-CNT@NiO electrode for high-performance asymmetric supercapacitor, a flexible full cell with GF-CNT@NiO as the cathode and graphene/carbon nanotube paper as the anode was fabricated (Details see Experimental Section). G-CNT paper anode was fabricated by vacuum filtrition of a graphene oxide/CNT solusion with a chemcial reduction followed. The corresponding SEM image and electrochemical behaviors of G-CNT paper are shown in Figure 4. Figure 4a-b show the SEM images of the G-CNT paper, from which one can see the paper is constructed with layed gaphenes and plenty of hollow space exists between the graphene layers. The hollow space will facilitae electrolyte penetration and ion transport.[2] Enlarged SEM image in Figure 4c clearly shows the CNT and graphene, further confirming the nanocomposite structure of the G-CNT paper. Electrochemical test results of G-CNT paper are presented in Figure 4d-f. The G-CNT paper shows a typical doule-layer behaviour, with a qusi-rectangular curve in CV test (Figure 4d). The EIS result also shows G-CNT paper has relatively low resistance for charge transfer and ion diffusion (Figure 4d). Further more, at a current density of 1 A g^{-1}, G-CNT anode can deliever a high capacitance of 129.2 F g^{-1}, and 80.3% of the capacity can be maintained when the current density is increased to 10 A g^{-1} (Figure 4f). These electrochemical results of G-CNT paper reveal that it is a good anode to be coupled with GF-CNT@NiO for high performance asymmetric supercapacitor.

Figure 5a shows the schematic structure of the GF-CNT@NiO//G-CNT asymmetric supercapacitor, where the two electrodes and electrolyte-absorbed seperator have been sandwiched between two PET plate. Figure 5b displays the CV curves of the GF-CNT@NiO//G-CNT cell at various scan rates in the voltage range of 0-1.6 V. A pair of redox peaks are observed at ~1.0 V and ~1.4 V, which correspond well with the previous results of NiO and carbon based hybrid supercapacitor, and the reaction here can be defined as the reverserable reaction with Ni^{2+} and OH^-.[46, 50] In Figure 5c, the asymmtric supercapacitor shows discharge voltage plateau from ~0.9 to ~1.3 V in galvanostatic charge/discharge test, which matches well with the CV curve. As shown in Figure 5c, the full-cell is charge-discharged in a short time range from 6 to 79.2 seconds, showing its ultrafast feature. Figure 5d displays the Ragone plots of the GF-CNT@NiO// G-CNT paper full cell, with some values from previously reported energy storage devices added for comparison purpose. Interestingly, the GF-CNT@NiO// G-CNT cell is able to deliever a high power density of 7.14 kW kg^{-1} at an energy density of 11.9 Wh kg^{-1}, and can hold a power density of 1.06 kW kg^{-1} at a high energy density of 23.4 Wh kg^{-1}, further demonstrating that the GF-CNT@NiO// G-CNT paper exhibits an outstanding rate capability. Considering the energy density and power density values are based on the whole electrode mass, these values are still larger with many of those reported NiO (and $Ni(OH)_2$) based asymmetric supercapacitors[21, 51] (a detailed comparison can be found in Electronic Supplementary Information). Indeed it has been challenging to achieve power densities of ~1-7 kW kg^{-1} for NiO or $Ni(OH)_2$ based electrodes. In addition, the energy/power density of the GF-CNT@NiO// G-CNT cell are also larger than many of the values reported for oxide-based asymmetric supercapacitors, such as MnO_2//Bi_2O_3[52], MnO_2-G//G[53], and CoO@PPy//AC[54]. Nevertheless, the G-CNT paper anode did not show very high capacitance (less than 150 F g^{-1}) but it accounted for 78.6% of the total electrode mass, thus it remains much room to further improve the power/energy density of the NiO based asymmetric supercapacitor by employing other high-capacitance anode materials.

As a key parameter to evaluate the supercapacitor performacne, the cycling ability test of the GF-CNT@NiO// G-CNT device was condcuted at a current of 4 A g^{-1}, as shown in in Figure 5e. Even after a long-time test of 30 000 cycles, ~81.7% of the initial capacity can be maintained, showing its excellent cycling ability. Furthermore, the coulombic efficiency is still close to 100% after the long-time testing, as shown in the insert of Figure 5e. The cycling behaviour of the GF-CNT@NiO// G-CNT is therefore much better than those of previously reported NiO or $Ni(OH)_2$ based supercapacitors. [21, 22, 46, 50, 55, 56] Based on the

results from the present study, the much improved cycling ability can be attributed to the followings: (i) the stable physichemical and mechanical connection between the refined metal oxide nanoparticles and CNTs enabled by ALD,[35] (ii) the crystalline metal oxides which enable fast redox reaction, (iii) the free space between the metal oxide nanoparticles to buffer the volume expansion/change,[57] and (iv) the GF-CNT structure and G-CNT paper which serves as stable support[58].

As discussed above, the GF-CNT@NiO// G-CNT full cell demonstrates excellent overall electrochemical properties, including high power density and excellent cycling ability, which is very promising for high-performance energy storage. As a demonstration for practical application, three full-cells (each contains 1*2 cm^2 of GF-CNT@NiO) can easily light up 9 parelalled LEDs, as shown in Figure 5f.

Conclusions

In conclusion, confined NiO nanoparticles have been assembled on a flexible carbon substrate (Graphite foam-CNT forest), which achieves very high specific capacity and excellent cycling ability, showing its promising usage as a battery-typed cathode material for asymmetric supercapacitors. By coupled with an anode material of a flexible G-CNT paper, a flexible binder-free and carbon additive-free asymmetric supercapacitor has been achieved. The asymmetric supercapacitor has demonstrated very high power densities (1.06-7.14 kW kg^{-1}) with high energy densities (11.9-23.4 Wh kg^{-1}) based on the total electrode mass, which is indeed much improved compared with those of other NiO based supercapacitors. Moreover, the GF-CNT@NiO// G-CNT cell exhibits exceptionally rate capability and excellent cycling stability that can retain more than 80% of the initial capacity after 30 000 cycles, which is among the best cycling performance achieved so far by a NiO-based device. The realization of the high power and durable NiO based asymmetric supercapacitor offers new opportunities for constructing high-performance energy-storage devices.

Method

Preparation of GF-CNT flexible substrate: GF-CNT hierarchical structure is fabricated by a two-step chemical vapor deposition (CVD) method,[29] where GF was obtained using commercial Nickel foam (8*8*0.2 cm^3) as substrate (with the Ni etched by 3M HCl) and CNT was grown on the GF using NiCo as the catalyst. The areal density of GF-CNT was adjusted to 0.65 mg cm^{-2}.

Preparation of GF-CNT@NiO: ALD NiO on GF-CNT was performed in a SUNALE R-200 ALD reactor (Picosun Oy). O_3 (Ozone concentration ~10%, generated in a 500 sccm mixture of oxygen (99.99%) and nitrogen (99.998%)) was used as the oxygen source, and Ni $(Cp)_2$ (held in a stainless steel bottle maintained at 125 ^oC) was used as the source for nickel. During the deposition process, the reaction chamber was maintained at 300 ^oC and ~13 hPa, and nitrogen (99.999%) was used as the carrying and purge gas. Each cycle contains a 1.6 s pulse time of nickel precursor with a 6 s purge time, and a 2 s O_3 precursor exposure time with a 5 s purge time. The mass loadings of GF-CNT@600NiO, GF-CNT@600NiO, and GF-CNT@600NiO are ~1.33, 1.53, and 1.88 mg cm^{-2}, respectively.

Preparation of G-CNT paper: GO aqueous solution (5 mg mL^{-1}) and CNT aqueous solution (3% mass content) were well mixed and vacuum filtered into a thin paper in the first step. The as-prepared paper was then reduced in a hydrazine solution (98%) at 70^oC for 0.5 h, and dried in vacuum oven in 60^oC.

Characterization: Samples were characterized using scanning electron microscopy (SEM, Zeiss, 5.0-20.0 kV), transmission electron microscopy (TEM, JEOL-2100F) with an EDX detector, X-ray photoelectron spectroscopy (XPS, AXIS Ultra), X-Ray Diffraction (XRD, Bruker D8 ADVANCE), and thermal gravimetric analysis (SDT Q600). The mass of electrode materials was also recorded by an AX/MX/UMX Balance (METTLER TOLEDO, maximum=5.1 g; delta= 0.001 mg).

Electrochemistry measurement: Solartron 1470E was used for all electrochemical test at room temperature. For three-electrode system tests, GF-CNT@NiO or G-CNT was directly used as the working electrode without any metal support or other current collector. A Pt plate and an Hg/HgO were used as the counter electrode and the reference electrode, respectively. KOH (2M) was used as the electrolyte. To assemble the full cell, GF-CNT@NiO, an electrolyte-soaked separator, and G-CNT paper were packed between two PET sheets and sealed with a Lacor home vacuum pack. The specific capacity of the electrode was calculated by $C=It/m$, where I is the discharge current, t is the discharge time, and m is the electrode mass. For the full cell assembly, to optimize the charge between the two electrodes, the mass of the two electrodes were balanced by $C_-m_-=C_+m_+$, where C_- and C_+ are the capacities of the negative and positive electrodes respectively, and m_- and m_+ are the masses of the negative and positive electrodes respectively. In a typical cell, the mass ration of GF-CNT@NiO to G-CNT paper is ~1.5:5.5. The energy density (E) and power density (P) of the full cell were calculated by: $E=\int_0^t IV(t)dt$, $P=E/t$, where I is the discharge current, V is the discharge voltage, t is the discharge time and m is the total mass of the electrodes.

Acknowledgements

This research is supported by the Ministry of Education (Singapore), Grant number: MOE2012-T2-2-102, conducted at the National University of Singapore. This work was also supported by MOE under AcRF Tier 2 (ARC 26/13, No. MOE2013-T2-1-034; ARC 19/15, No. MOE2014-T2-2-093) and AcRF Tier 1 (RGT18/13, RG5/13), NTU under Start-Up Grant (M4081296.070.500000) and iFood Research Grant (M4081458.070.5000000), and Singapore Millennium Foundation in Singapore. This research grant is supported by the Singapore National Research Foundation under its Environmental & Water Technologies Strategic Research Programme and administered by the Environment & Water Industry Programme Office (EWI) of the PUB. This Research is also conducted by NTU-HUJ-BGU Nanomaterials for Energy and Water Management Programme under the Campus for Research Excellence and Technological Enterprise (CREATE), that is supported by the National Research Foundation, Prime Minister's Office, Singapore.

Notes and references

1. P. Simon, Y. Gogotsi and B. Dunn, *Science*, 2014, **343**, 1210-1211.
2. X. Cao, Z. Yin and H. Zhang, *Energy & Environmental Science*, 2014, **7**, 1850-1865.
3. X. Lu, M. Yu, G. Wang, Y. Tong and Y. Li, *Energy & Environmental Science*, 2014, **7**, 2160-2181.
4. H. Wang and H. Dai, *Chemical Society Reviews*, 2013, **42**, 3088-3113.
5. V. Augustyn, P. Simon and B. Dunn, *Energy & Environmental Science*, 2014, **7**, 1597-1614.
6. M. Zhi, C. Xiang, J. Li, M. Li and N. Wu, *Nanoscale*, 2013, **5**, 72-88.
7. J. Jiang, Y. Li, J. Liu, X. Huang, C. Yuan and X. W. Lou, *Advanced Materials*, 2012, **24**, 5166-5180.
8. L. Peng, X. Peng, B. Liu, C. Wu, Y. Xie and G. Yu, *Nano Letters*, 2013, **13**, 2151-2157.
9. G. Wang, L. Zhang and J. Zhang, *Chemical Society Reviews*, 2012, **41**, 797-828.
10. Z. Zhu, J. Ping, X. Huang, J. Hu, Q. Chen, X. Ji and C. Banks, *Journal of Materials Science*, 2012, **47**, 503-507.
11. Z. Lu, Z. Chang, W. Zhu and X. Sun, *Chemical Communications*, 2011, **47**, 9651-9653.
12. X. Xia, Y. Q. Zhang, D. Chao, G. Cao, Y. Zhang, L. Li, X. Ge, I. M. Bacho, J. Tu and H. J. Fan, *Nanoscale*, 2014, **6**, 5008-5048.
13. X. Wang, X. Li, X. Sun, F. Li, Q. Liu, Q. Wang and D. He, *Journal of Materials Chemistry*, 2011, **21**, 3571-3573.
14. H. Jiang, C. Li, T. Sun and J. Ma, *Chemical Communications*, 2012, **48**, 2606-2608.
15. S. A. Needham, G. X. Wang and H. K. Liu, *Journal of Power Sources*, 2006, **159**, 254-257.
16. H. Wang, H. S. Casalongue, Y. Liang and H. Dai, *Journal of the American Chemical Society*, 2010, **132**, 7472-7477.
17. W. Chen, C. Xia and H. N. Alshareef, *ACS Nano*, 2014, **8**, 9531-9541.
18. C. Wang, F. Li, H. Qu, Y. Wang, X. Yi, Y. Qiu, Z. Zou, Y. Luo and B. Yu, *Electrochimica Acta*, 2015, **158**, 35-41.
19. M. Chen, L. Zhang, S. Duan, S. Jing, H. Jiang and C. Li, *Advanced Functional Materials*, 2014, **24**, 7548-7556.
20. W. Feng, M. Qin, P. Lv, J. Li and Y. Feng, *Carbon*, 2014, **77**, 1054-1064.
21. J. Yan, Z. Fan, W. Sun, G. Ning, T. Wei, Q. Zhang, R. Zhang, L. Zhi and F. Wei, *Advanced Functional Materials*, 2012, **22**, 2632-2641.
22. Z. Tang, C.-h. Tang and H. Gong, *Advanced Functional Materials*, 2012, **22**, 1272-1278.
23. X. Zhang, W. Shi, J. Zhu, W. Zhao, J. Ma, S. Mhaisalkar, T. Maria, Y. Yang, H. Zhang, H. Hng and Q. Yan, *Nano Research*, 2010, **3**, 643-652.
24. Z. Li, Z. Xu, H. Wang, J. Ding, B. Zahiri, C. M. B. Holt, X. Tan and D. Mitlin, *Energy & Environmental Science*, 2014, **7**, 1708-1718.
25. H. Wang, C. B. Holt, Z. Li, X. Tan, B. Amirkhiz, Z. Xu, B. Olsen, T. Stephenson and D. Mitlin, *Nano Research*, 2012, **5**, 605-617.
26. X. Xiao, T. Ding, L. Yuan, Y. Shen, Q. Zhong, X. Zhang, Y. Cao, B. Hu, T. Zhai, L. Gong, J. Chen, Y. Tong, J. Zhou and Z. L. Wang, *Advanced Energy Materials*, 2012, **2**, 1328-1332.
27. J. Xu, Q. Wang, X. Wang, Q. Xiang, B. Liang, D. Chen and G. Shen, *ACS Nano*, 2013, **7**, 5453-5462.
28. J.-H. Kim, S. H. Kang, K. Zhu, J. Y. Kim, N. R. Neale and A. J. Frank, *Chemical Communications*, 2011, **47**, 5214-5216.
29. j. liu, L. L. Zhang, H. Wu, J. Lin, Z. Shen and D. X.-W. Lou, *Energy & Environmental Science*, 2014, **7**, 3709-3719.
30. X. Tong, Y. Qin, X. Guo, O. Moutanabbir, X. Ao, E. Pippel, L. Zhang and M. Knez, *Small*, 2012, **8**, 3390-3395.
31. H. L. Lu, G. Scarel, C. Wiemer, M. Perego, S. Spiga, M. Fanciulli and G. Pavia, *Journal of The Electrochemical Society*, 2008, **155**, H807-H811.
32. C. Marichy, M. Bechelany and N. Pinna, *Advanced Materials*, 2012, **24**, 1017-1032.
33. X. Meng, X.-Q. Yang and X. Sun, *Advanced Materials*, 2012, **24**, 3589-3615.
34. C. Chen, C. Chen, P. Huang, F. Duan, S. Zhao, P. Li, J. Fan, W. Song and Y. Qin, *Nanotechnology*, 2014, **25**, 504001.
35. C. Guan, J. Liu, Y. Wang, L. Mao, Z. Fan, Z. Shen, H. Zhang and J. Wang, *ACS Nano*, 2015, **9**, 5198-5207.
36. S. Oswald and W. Brückner, *Surface and Interface Analysis*, 2004, **36**, 17-22.
37. C. Guan, Y. Wang, M. Zacharias, J. Wang and H. J. Fan, *Nanotechnology*, 2015, **26**, 014001.
38. B. Varghese, M. V. Reddy, Z. Yanwu, C. S. Lit, T. C. Hoong, G. V. Subba Rao, B. V. R. Chowdari, A. T. S. Wee, C. T. Lim and C.-H. Sow, *Chemistry of Materials*, 2008, **20**, 3360-3367.
39. J. Zhu, J. Jiang, J. Liu, R. Ding, H. Ding, Y. Feng, G. Wei and X. Huang, *Journal of Solid State Chemistry*, 2011, **184**, 578-583.
40. C. Yuan, X. Zhang, L. Su, B. Gao and L. Shen, *Journal of Materials Chemistry*, 2009, **19**, 5772-5777.
41. Z.-H. Gao, H. Zhang, G.-P. Cao, M.-F. Han and Y.-S. Yang, *Electrochimica Acta*, 2013, **87**, 375-380.
42. J. Li, W. Zhao, F. Huang, A. Manivannan and N. Wu, *Nanoscale*, 2011, **3**, 5103-5109.
43. C. Guan, X. Qian, X. Wang, Y. Cao, Q. Zhang, A. Li and J. Wang, *Nanotechnology*, 2015, **26**, 094001.
44. T. Brousse, D. Bélanger and J. W. Long, *Journal of The Electrochemical Society*, 2015, **162**, A5185-A5189.
45. C.-Z. Yuan, B. Gao and X.-G. Zhang, *Journal of Power Sources*, 2007, **173**, 606-612.
46. J. Ji, L. L. Zhang, H. Ji, Y. Li, X. Zhao, X. Bai, X. Fan, F. Zhang and R. S. Ruoff, *ACS Nano*, 2013, **7**, 6237-6243.
47. F. Luan, G. Wang, Y. Ling, X. Lu, H. Wang, Y. Tong, X.-X. Liu and Y. Li, *Nanoscale*, 2013, **5**, 7984-7990.
48. C. Guan, X. Xia, N. Meng, Z. Zeng, X. Cao, C. Soci, H. Zhang and H. J. Fan, *Energy & Environmental Science*, 2012, **5**, 9085-9090.
49. C. Guan, J. Liu, C. Cheng, H. Li, X. Li, W. Zhou, H. Zhang and H. J. Fan, *Energy & Environmental Science*, 2011, **4**, 4496-4499.
50. H. Wang, H. Yi, X. Chen and X. Wang, *Journal of Materials Chemistry A*, 2014, **2**, 3223-3230.
51. J.-W. Lang, L.-B. Kong, M. Liu, Y.-C. Luo and L. Kang, *J Solid State Electrochem*, 2010, **14**, 1533-1539.
52. H. Xu, X. Hu, H. Yang, Y. Sun, C. Hu and Y. Huang, *Advanced Energy Materials*, 2014, **5**, n/a-n/a.
53. Z.-S. Wu, W. Ren, D.-W. Wang, F. Li, B. Liu and H.-M. Cheng, *ACS Nano*, 2010, **4**, 5835-5842.
54. P. Cai, D.-K. Ma, Q.-C. Liu, S.-M. Zhou, W. Chen and S.-M. Huang, *Journal of Materials Chemistry A*, 2013, **1**, 5217-5223.

55. H. B. Li, M. H. Yu, F. X. Wang, P. Liu, Y. Liang, J. Xiao, C. X. Wang, Y. X. Tong and G. W. Yang, *Nat Commun*, 2013, **4**, 1894.
56. J.-H. Kim, K. Zhu, Y. Yan, C. L. Perkins and A. J. Frank, *Nano Letters*, 2010, **10**, 4099-4104.
57. X. Lai, J. E. Halpert and D. Wang, *Energy & Environmental Science*, 2012, **5**, 5604-5618.
58. J. Liu, M. Chen, L. Zhang, J. Jiang, J. Yan, Y. Huang, J. Lin, H. J. Fan and Z. X. Shen, *Nano Letters*, 2014, **14**, 7180-7187.

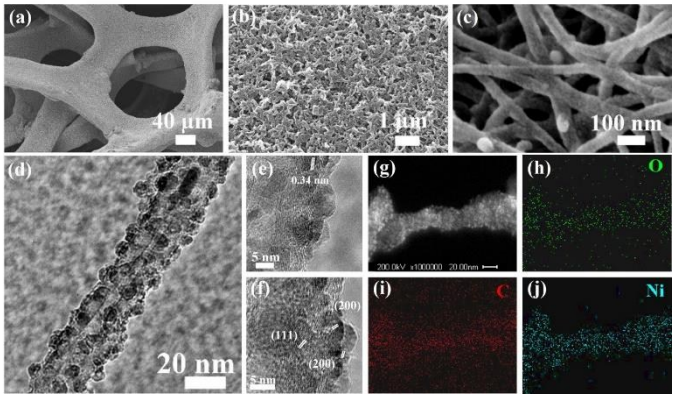

Figure 1. SEM and TEM characterization of GF-CNT@NiO. (a-c) SEM and (d-f) HRTEM images of GF-CNT@NiO. (g) HAADF-STEM image of CNT@NiO, and (h-j) the corresponding STEM element mapping results.

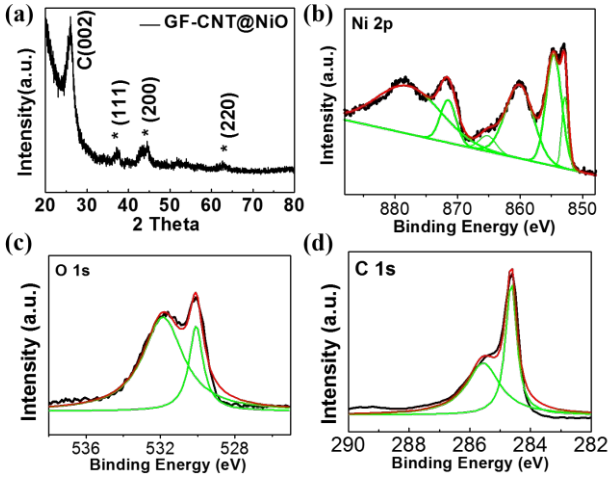

Figure 2. Characterization of GF-CNT@NiO. (a) XRD and (b-d) XPS results of GF-CNT@NiO.

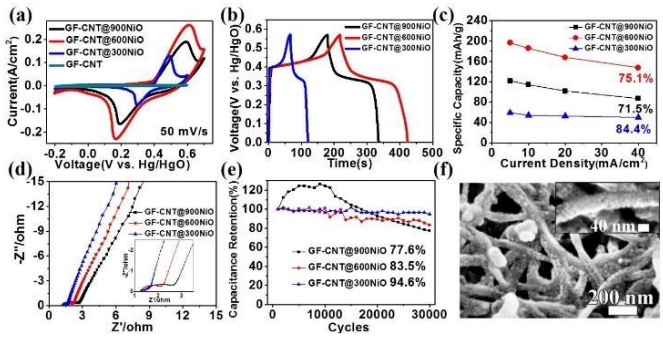

Figure 3. Electrochemical performance of GF-CNT@NiO: (a) CV curves, (b) charge-discharge curves, (c) rate capability, (d) EIS, and (e) cycling ability of the three samples: GF-CNT@300NiO, GF-CNT@600NiO, and GF-CNT@900NiO. The number in (c) shows the capacity retention when the current increased from 5 to 40 mA cm^{-2}, and the number in (e) shows the capacity retention after 30 000 cycles. (f) SEM images for GF-CNT@600NiO after 30 000 cycles.

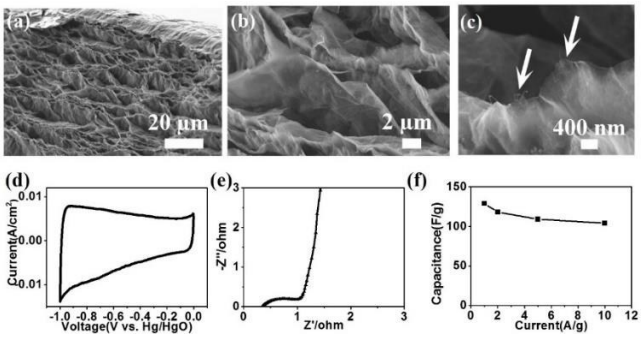

Figure 4. G-CNT paper as the anode material. (a-c) SEM images of G-CNT paper. (d) CV curve, (e) EIS, and (f) rate capability of G-CNT paper. Arrows in (c) show the CNTs in the composite paper.

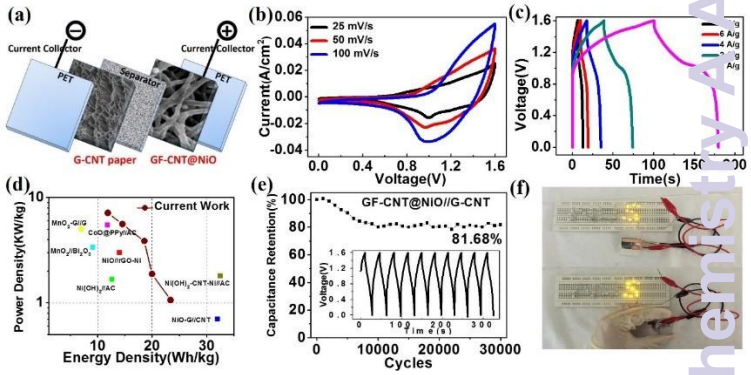

Figure 5. Electrochemical behaviour of the GF-CNT@NiO // G-CNT full-cell. (a) Schematic of the full-cell package. (b) CV curves, (c) charge-discharge curves, (d) Ragone plot, and (e) cycling ability of the GF-CNT@NiO // G-CNT. Some values reported from other ASCs are inserted in (d) for comparison purpose. Insets in (e) shows the 10 charge-discharge curves after 30 000 cycles. (f) The digital photos that a set of 3 cells can light up 9 orange LEDs.